Local microstructural characterization of an aged UR45N rolled steel: Application of the nanogauges grating coupled EBSD technique

Joseph Marae Djouda, Benoît Panicaud, Fabrice Gaslain, Jérémie Béal, Yazid Madi, Guillaume Montay, Léa Le Joncour, Julien Gardan, Naman Recho, Jérôme Crépin, et al.

HAL Id: hal-02279180
https://utt.hal.science/hal-02279180

Submitted on 25 Oct 2021

Local microstructural characterization of an aged UR45N rolled steel: Application of the nanogauges grating coupled EBSD technique.

Joseph Marae Djouda[1, 2, 3], Benoît Panicaud[1],Fabrice Gaslain[4], Jérémie Beal[2], Yazid Madi[3, 4] Guillaume Montay[1], Léa Le Joncour[1], Julien Gardan[3], Naman Recho[3], Jérôme Crépin[4], Thomas Maurer[2].

[1]*Laboratoire des Systèmes Mécaniques et d'Ingénierie Simultanée, ICD CNRS FRE2019, Université de Technologie de Troyes, CS 42060, 10004 Troyes, France*
[2]*Lumière, Nanomatériaux, Nanotechnologies (L2n), Institut Charles Delaunay (ICD) CNRS FRE 2019, Université de Technologie de Troyes, CS 42060, 10004 Troyes, France*
[3]*ERMESS, EPF- Ecole d'ingénieurs, 3 bis rue Lakanal 92 330 Sceaux, France*
[4]*Centre des Matériaux, UMR CNRS 7633, BP 87, 91003 Evry Cedex, France*

Abstract:

In the present article, metallic nanoparticles (NPs) used as nanogauges and electron backscattered diffraction (EBSD) are combined to investigate deformation mechanisms of the UR45N duplex steel. The kinematic fields bring precious details in the evolution of the local deformation of austenitic and ferritic phases. The crystallographic information at the initial stage and in the plastic domain is obtained by the EBSD technique. Strain evolutions in each phase are analysed. The first strain marks appear in austenite just before the elastoplastic transition. Slip and twinning activities in austenite constitute an important part of the work hardening of the material. The slips in ferrite are visible in the plastic domain and present complex geometry. The role of phase boundaries, which act as strain barrier is highlighted. The incompatibilities of deformations between the two phases modify the deformation mechanism of austenite in comparison with a pure austenitic stainless steel as 316L. Local interactions between phases during the deformation are analysed. The strong strain heterogeneities in the plastic domain are analysed in the kinematic fields. Local evolutions of the deformation are also confronted to the macroscopic behaviour of the material.

Introduction:

Dual phase stainless steels also called duplex steels present two phases: ferrite and austenite. They are used in several industrial applications because of their mechanical properties. Indeed, they take advantages of the combination of the ductile feature and the high strength of austenitic and ferritic phases respectively. The comprehension of the evolution of the microstructure during mechanical loading is of great importance. The microstructure of duplex alloys has been studied during fatigue loadings (Aubin, 2006; Bugat, 2000; El Bartali et al., 2008) and in uniaxial tensile tests (Jia et al., 2008; Joncour et al., 2010). These studies have highlighted the heterogeneities of plasticity at the phases scale. The initiation and evolution of damage, as well as the propagation of micro-cracks have been studied in plastic fatigue (El Bartali et al., 2008). El Bartali and co-workers showed the activated slip systems in each phase. To carry out their works, they combined analyzes of in-situ image correlation during a fatigue test with Electron Backscattered Diffraction (EBSD) mapping of the specimen surface recorded at the initial state. More recently, Le Joncour and coworkers have implemented neutron and X-rays diffraction to follow the evolution of the elastic

deformations for different crystalline {hkl} planes in each phase (Zhao et al., 2017). However, very few studies have focused on the strain quantification at the local scale in order to understand the evolution of the microstructure deformation of such materials. Because of the presence of the two phases, it is crucial to study the evolution of the local deformation at the microscopic scale in each phase and at their interface. In this study, metallic nanoparticles (NPs) are used as nanogauges and allow the local quantification of displacements within the microstructure. The microstructure and the crystallographic orientations evolutions are analyzed related to the macroscopic behavior during a uniaxial tensile test. The initiation of strain mechanism in the austenitic phase is thus clearly brought out. This result has been demonstrated in several works and has been explained by the difference in hardness of the two phases in presence (Fréchard et al., 2006). Deformations in the ferritic phase, which presents the highest hardness, are often observed later for high strain levels. Displacements of NPs observed in the Scanning Electron Microscopy (SEM) images provide qualitative information on the progressive evolution of the deformations at the grain scale, and allow a first simple analysis of the local behavior (Clair et al., 2011; Marae Djouda et al., 2017; Maurer et al., 2015). The kinematic fields obtained from the SEM images then make it possible a quantification of these strains. The evolution of strains in each phase and at the interface between both phases has been analyzed. The EBSD technique provides information on the morphological and crystallographic texture in the area of the grating. Different EBSD acquisitions, made at specific loading level, allow the analysis of crystallographic evolutions. The kinematic field evolutions coupled to the crystallographic measurements thus make possible to identify the local mechanisms of deformations. In the following, the evolution of the kinetic fields and the texture are compared with the macroscopic behavior of the material.

1. Experiment

1.1. Presentation of the test

Figure 1a shows the specimen geometry used the in-situ tensile test. The specimen has been "mirror" polished for high quality EBSD acquisitions. The nanogauges grating consisted in gold nanocylinders with 200 nm diameter, 400 nm centre to centre separation in the same direction (square grating) and 50 nm in height has been deposited at the centre of the specimen by electron beam lithography (EBL). The grating dimensions are 70 µm * 70 µm (see Figure 1b. Once the specimen prepared, the crystallographic acquisition in the region containing the nanoparticles (NPs) array has been realized. The in-situ tensile test has been then proceeded and SEM images of the grating have been progressively recorded during the test at different loading levels. At the elasto-plastic transition, the applied force has been decreased to zero. The specimen has been removed, a second EBSD acquisition has been then performed. After this EBSD acquisition, the specimen has been loaded in order to reach the previous applied force. The speed of the displacement gauge of the micro-machine during the test has been 3.3 µm / s. The SEM images have been recorded again until the strain localization at the macroscopic scale has been approached. Then another discharge and a third EBSD acquisition has been then performed. At the end of the EBSD acquisition, the test has been conducted until the specimen failure. The summary of the different steps of the test is presented in Figure 1c. "Part I", is the part consisting of the first EBSD acquisition (EBSD_0), SEM images until the first discharge. "Part II" is the part consisting of the second EBSD acquisition (EBSD_1) and the SEM images until the second discharge. And "Part III" is the part consisting of the third EBSD acquisition (EBSD_2) and SEM images until the specimen

failure. A relaxation of the applied stress has been observed during the SEM images recording in the plastic domain, with values between 20 and 50 MPa (see Figure 1c). Similar observations have been reported by Aubin (Aubin, 2006) using a speed jump tensile, which highlighted the viscous nature of this alloy responsible for relaxation at room temperature. The relaxation phenomenon observed during tensile tests at the pause of the loading influences the material behavior and also depends on the hardening and on the induced transformations (Hariharan et al., 2013).
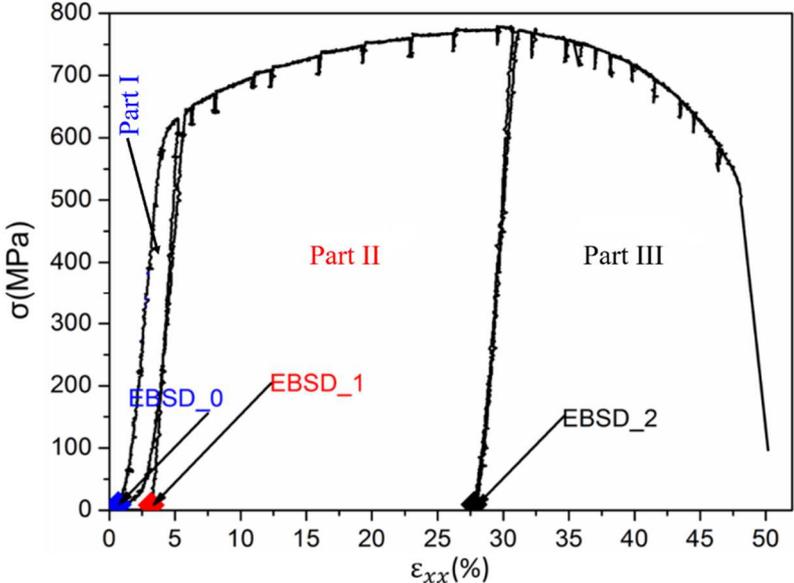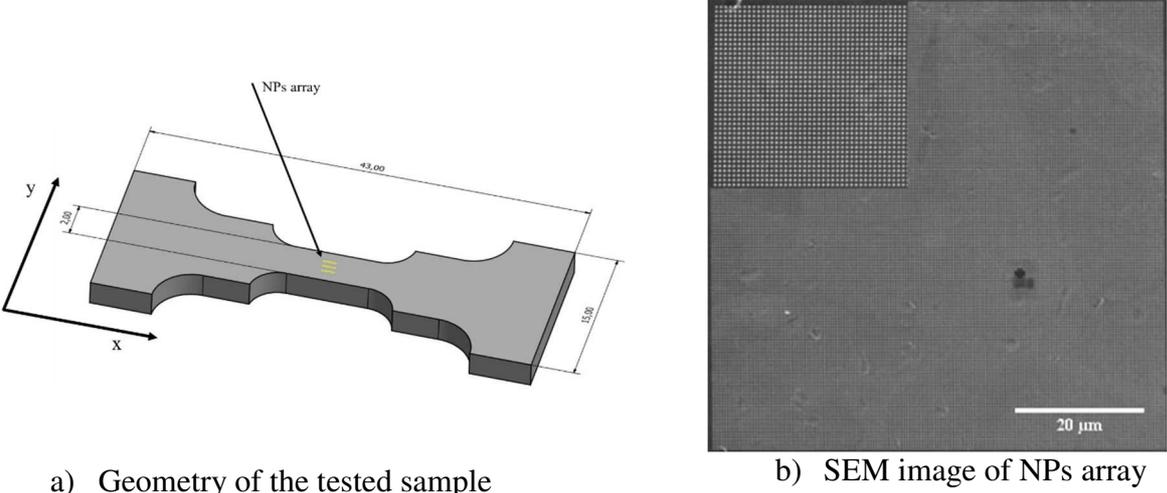

a) Geometry of the tested sample

b) SEM image of NPs array

c) Stress- strain curve of the specimen with the different parts of the test.

Figure 1: a) Geometry of the sample, the tensile direction is $\vec{x}$, b) SEM image of the sample and c) summary of the test showing the three considered parts.

1.2. Microstructure of the zone of interest

In order to analyze the local strains in the phases, the phase distribution in the area of the grating is presented at the initial state (see Figure 2a). The austenitic phase is shown in red and the ferritic one in green. A small ferritic band is located between two islands of austenitic phase in the region of interest. The twins due to the thermomechanical treatment in the

austenitic phase are numbered on the phase distribution map (see Figure 2a). They will be called "annealing twins" in the rest of article. The grains of this phase are also numbered in the inverse pole figure (Figure 2b). The annealing twins 1 and 5 have parent grains (which are the grains 7 and 11 respectively). Grains 1 and 4 are large enough and have an average surface area of 760 µm² and the rest of the grains have an average surface area around 130 µm². The ferritic band has very large grains. Similar observations of grain sizes have been obtained for similar materials by other authors (Wroński et al., 2012; Zhao et al., 2016).

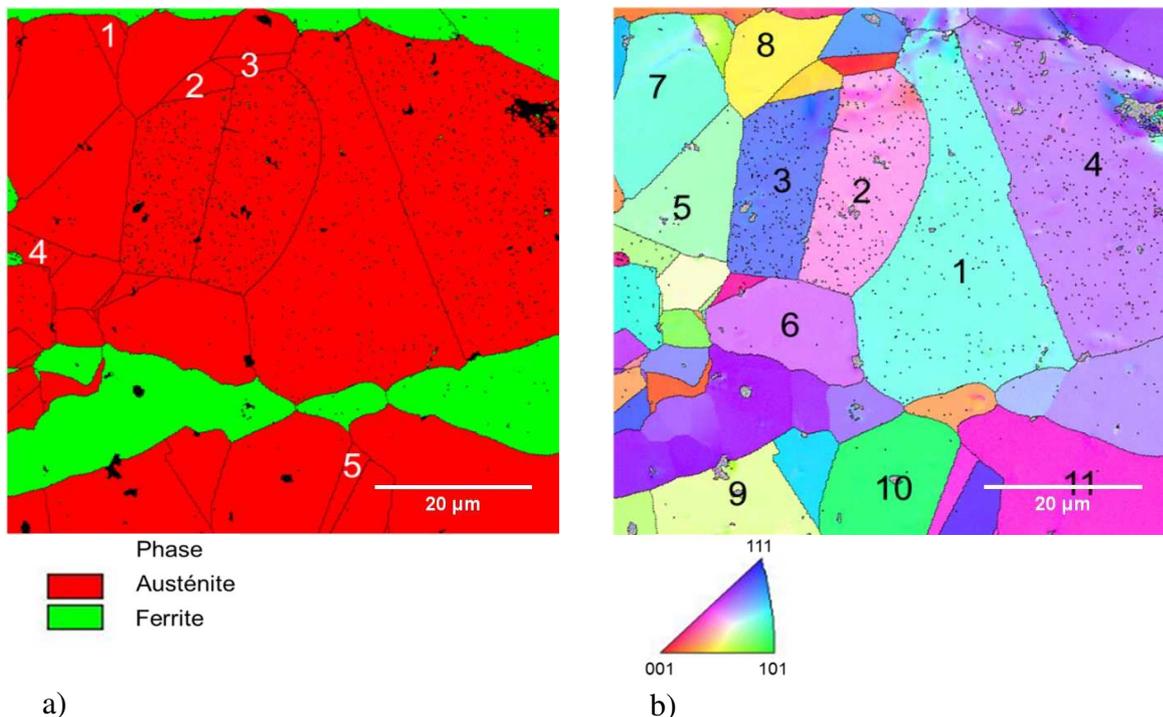a)   b)

Figure 2: a) Phase distribution and b) crystallographic orientations of the microstructure component in the area of the grating.

2. Microstructure evolution from SEM images

The size of the NPs and the pitch value of the grating make possible to locally monitor the deformations on the microstructure. The SEM images highlight the variations of the NP positions, which is assumed to directly reflect the deformations of the substrate in response to the applied loading. Neighboring NPs, which are initially well aligned, can form distortion lines when the specimen is submitted to a mechanical load (see Figures 3, 4 and 5). These distortions are due to local deformations of the microstructure components that can rotate through each other. The tracking of displacements and distortions of the lines of NPs with the loading thus allows a first comprehension of the local deformation evolutions.

During the loading, at the specimen surface, appears slip marks, grain elongations and rotations, and cracks at the boundaries or at the surface of the grains. As mentioned above, the test has been divided into three parts in order to facilitate the analysis. During the test, many SEM images have been recorded, however for the interpretation of the evolutions of

phenomenon during the test, only few images are presently shown. The local phenomena are highlighted as much as possible.

2.1. Part I of the test

Figure 3 shows some SEM images of the Part I of the test. The image corresponding to the loading level "i" is denoted by "T_i"; the image taken at the initial state before the application of any loading is called T_0. The arrow drawn on this image indicates a lithography defect, due to the presence of fine gas bubbles that have not been evaporated inside the PMMA resin, which may happen during the lithography process. Part I of the test corresponds macroscopically to the elastic domain up to the elastoplastic transition. The displacements of NPs first appear locally at some grains surface. These NPs displacements result in a difference of gray levels at the SEM image and variations of NPs positions. The NPs positions variations is evidence by straight lines, which constitute the slip marks. They are visible from loading level T_15 (see Figure 3). The first slip marks are visible later at loading level T_19 on the lower part of the grating. As the loading increases, these marks become more visible and new slip marks appear progressively on other grains. These slips probably result from the dislocations motion in the volume of the material (Morgeneyer et al., 2014). It is important to notice that at this stage all these slips belong to the austenitic phase. The macroscopic stress corresponding to the loading level of image T_19 is around 540 MPa. At this level, the material still exhibits an elastic behavior at the macroscopic level. Between the loading levels T_19 and T_22, the relative displacements of the NPs increase locally at the first slip marks and in their neighboring, new slip marks appear.

2.2. Part II of the test

The second part of the test corresponds macroscopically to the plastic domain. Figure 4 shows some SEM images of this part. At T_25, the population of slips increases at the surface of austenitic grains. The strain intensity at grain boundaries of the austenitic phase is important and they present some visible cracks (see Figure 4). However, it seems that these cracks do not come from the volume of the material. As the loading increases from T_25 to T_28, the crack propagates to the triple point; it continues along the initial joint and is oriented towards the neighboring grain boundaries in austenite. The zoom of this crack around the triple point is shown in Figure 4. The grain boundary (1) belongs to the austenitic phase and the boundaries (2) and (3) are related to phase boundary (junction between the austenitic and ferritic phases). The intensity of the strain around grain boundaries and on the adjacent grain increases (grain 4). It appears that some regions of the specimen surface present a large number of slips marks with high strain intensity, while others remain with very low or no slip activity. These lasts correspond to ferrite. Because of it important strength value, ferrite enters in plasticity later than austenite (Joncour et al., 2010). A strain concentration is observed at the slip marks of the grains, which belong to these boundaries. The important slip activity in the austenitic phase seems to accumulate strains at the phase boundary.

Slip activity in the ferritic phase is visible from loading level T_28. It is accompanied by a clear visualization of grain contours and triple points. The difference in topography at the surface of the sample is also remarkable. Slip marks in the ferritic phase also increase with the loading, but the population of these slips is relatively low compared to the one in austenitic phase. However, they present a specific geometry, they are curved ("sinuous") and have relative width. The strains concentrated at the phase boundaries now evolve between both

phases as the loading increases. It means that the slip marks stopped at the phase boundaries now move from the austenitic phase to the ferritic phase (see the zoom of the SEM_T_33, Figure 4). From these observations, the phase boundaries act as strain barriers. At these barriers, the slip marks of the austenitic phase are stopped and accumulated when the load increases. For a specific threshold, the barriers are no more efficient and then slip marks can move from one phase to another. The failure of the barriers seems to be favored by the activation of the deformation of the ferritic phase. The phase boundary, which react as strain barrier could be deformed enough due to the incompatibility of deformations.
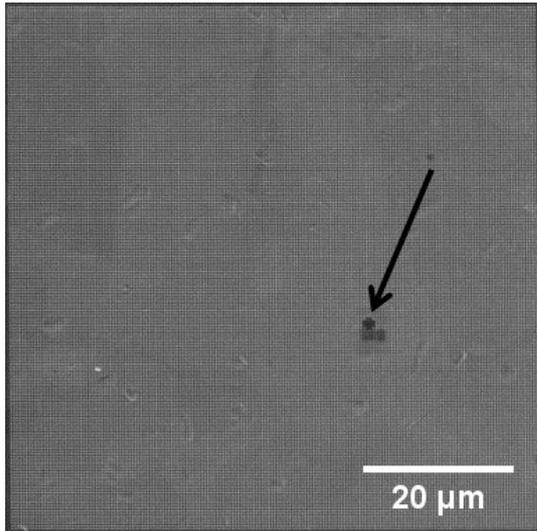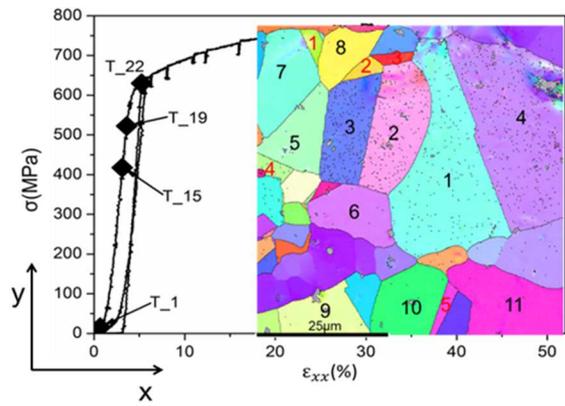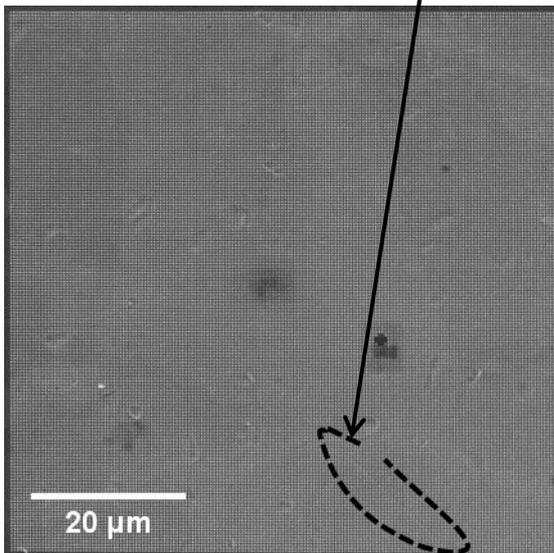
T_0 : Grating of NPs at initial level
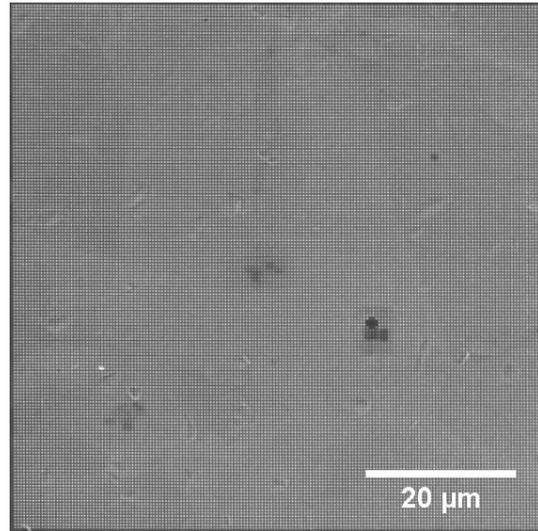
T_15 : Strain initiation
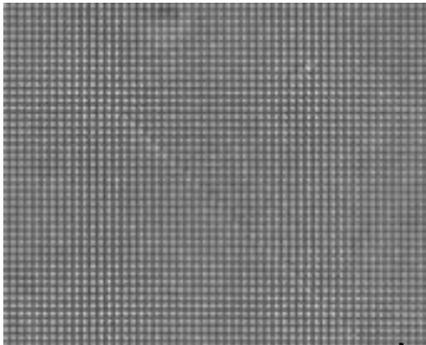
Highlight of the slip marks

Macroscopic behaviour of the material

T_19 : Slip marks appearance
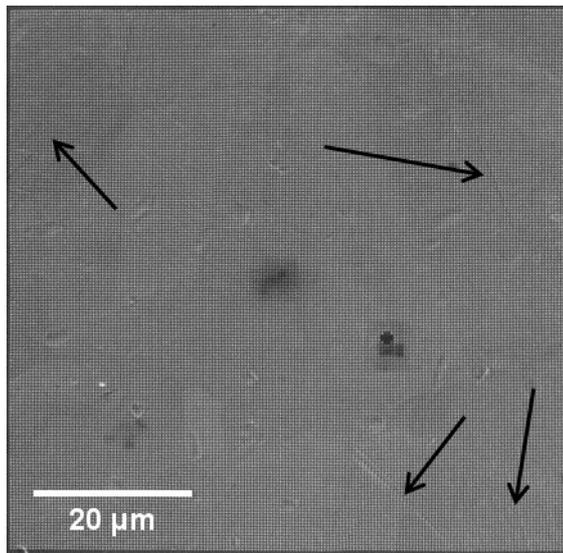
T_22 : Increased of slip marks population

Figure 3: Strains observation on the microstructure using the displacements of the NPs on the part I of the test.
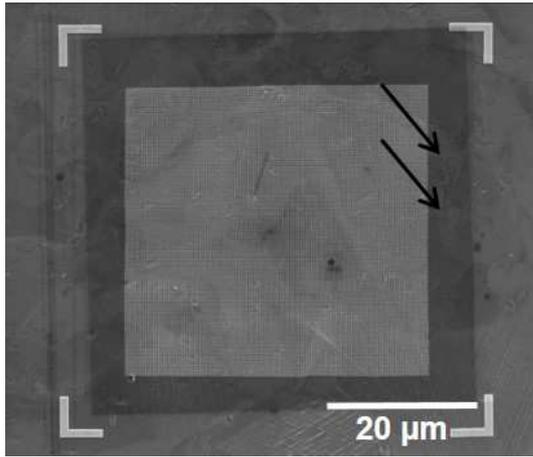
T_25 : Strain increased at the grain boundaries
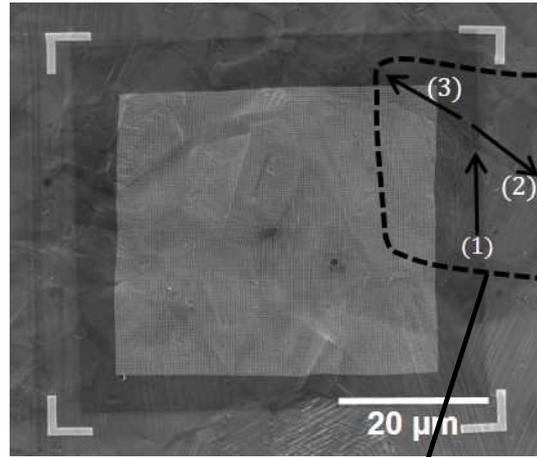
T_28 : Increased of strains at slip marks
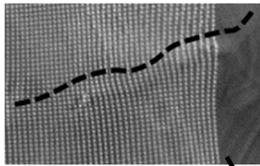
Phase boundary

Macroscopic behaviour of the material
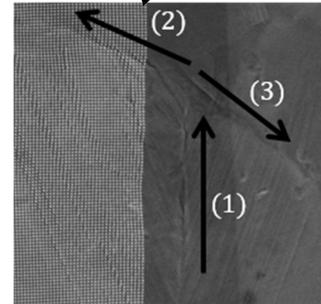
Triple junction
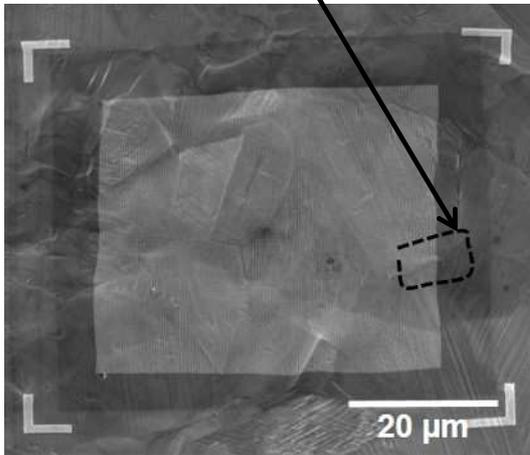
T_31 : Deformation at the phase boundary
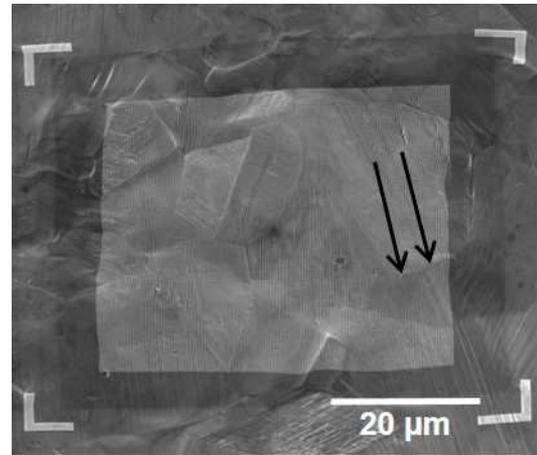
T_33 : Continuity of deformation between phases

Figure 4: Strains observation on the microstructure using the displacements of the NPs on the part II of the test.
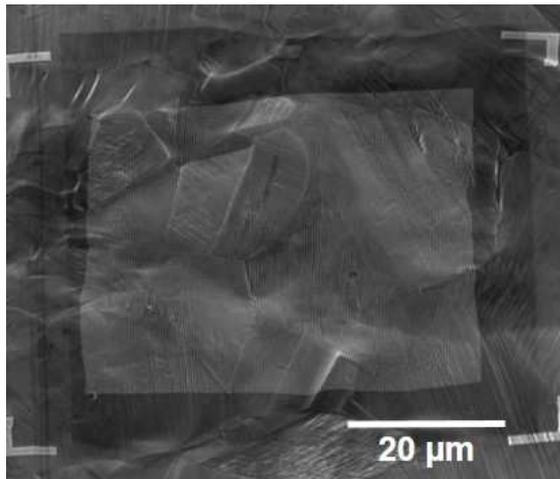
T_36 : Evolution of strain heterogeneities
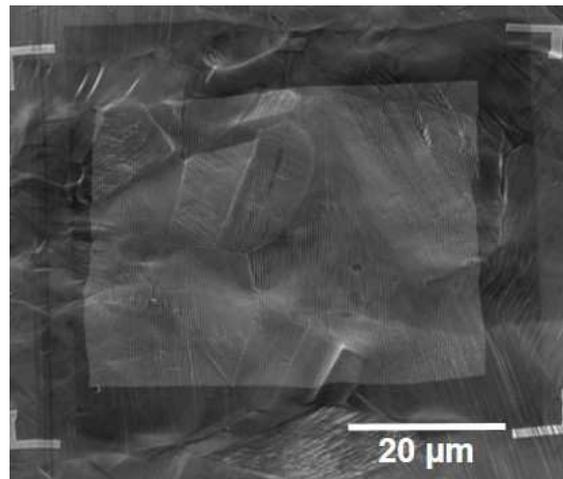
T_39
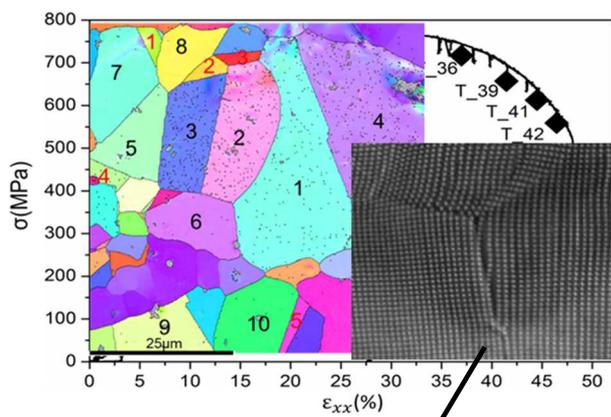
Macroscopic behaviour of the material
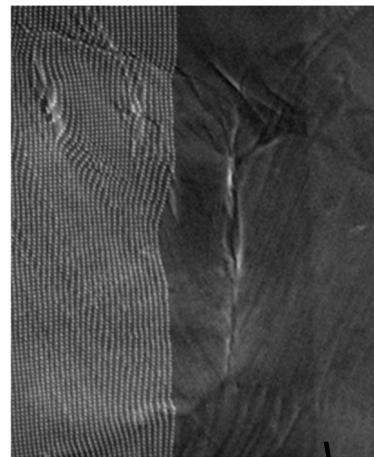
Strain evolution at the boundaries
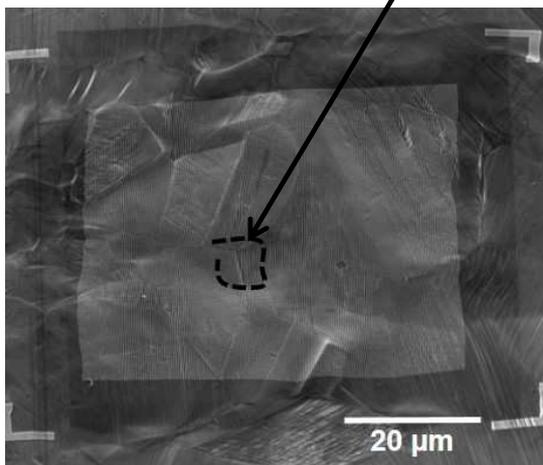
T_41
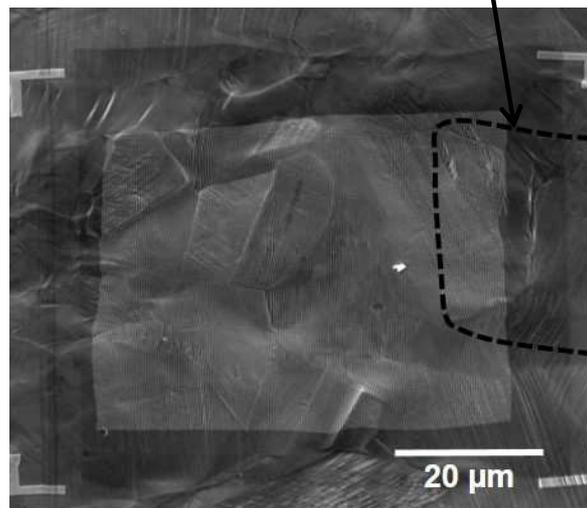
T_42 : Microstructure just before the failure

Figure 5: Strains observation on the microstructure using the displacements of the NPs on the part III of the test.

2.3. Part III of the test
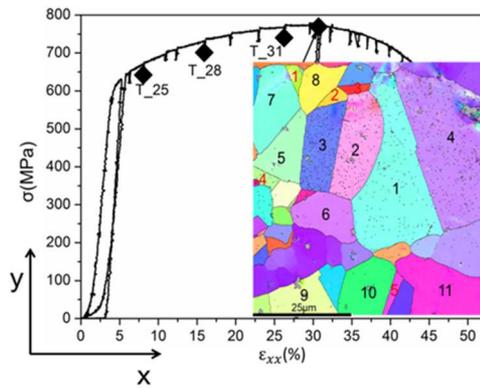
The part III of the test is macroscopically related to the cross section reduction and the necking of the specimen. Heterogeneities of deformations become more and more marked at different microstructure components. Another phenomenon is visible at the specimen surface: the strain concentrations at the triple points, with strain intensity increasing at the grains and phase boundaries. Figure 5 presents all these evolutions on some SEM images corresponding to this part. It can be seen in Fig. 5 that some austenite grains have a rough appearance due to cross-slips, while others grains changed orientation and are stretched strongly in the tensile direction. The crack at the triple point in the austenitic phase moves in the ferritic phase in two different directions from T_36. It then appears that the features at the triple point in the austenitic phase strongly influence the deformation of the microstructure. For example, at the first triple point in the austenitic phase, three grain boundaries have been simultaneously opened. The deformation and the crack at these boundaries increase during the loading and the crack (1) continues toward the phase boundary. It is worth noting that despite the NPs grating has been deposited at the specimen center, the failure position has been located at 3.5 mm from the middle. The SEM image showing the relative position of the grating to the failure is presented in Supporting Information (SI).

Once the SEM images with the NPs positions at different loading levels are obtained, it is now possible to access to the strain maps of the area of the grating, as already processed in previous works (Marae Djouda et al., 2018, 2017). The NPs play the role of the nanogauges and then allow strain quantification. These strain maps combined with the crystallographic information of the material give precious details for the understanding of the material behavior (Marae Djouda et al., 2018). This constitutes a robust approach to study the materials behavior. In the following sections, the strain maps obtained from the SEM images are presented and the analysis is led for the material study herein.

3. Analysis of 2D strain maps

The SEM images give a comprehensive but qualitative evolution of microstructure deformation. However, to go forward in the analysis, it is important to get the local quantification of the strain at the microstructure. The strain quantification can be shown on the strain maps of the Euler-Almansi tensor components ε_{xx} ε_{xy} and ε_{yy} (Marae Djouda et al., 2017). In the following, the strain evolution in the tensile direction is systematically presented for the component ε_{xx}. The strain maps were superimposed with the grain image from EBSD in order to allow an easy correlation of strain with crystallographic information. The strain maps corresponding to the others components; ε_{xy} and ε_{yy} are presented in the SI.

3.1. Analysis of ε_{xx} : Part I of the test

3.1.1. Deformations in the austenitic phase

In Figure 6, it must be noted that the color bars are not homogeneous for all the images: T_1 and T_15 levels have their color bars in [0 – 3] % bracket while that of the T_19 and T_22 levels is in [0 – 5] % bracket. This choice should help highlighting the local strain evolutions. The deformations are homogeneously distributed on the specimen surface and present very low values (less than 1%) up to the loading level T_15 ($\sigma < 500\,\mathrm{MPa}$). By increasing the loading, first slip marks appear at the specimen surface, the strain distribution

at large grains specifically are not null (T_19, Figure 4). The first deformation marks are then visible for macroscopic stress around $\sigma = 540$ MPa. The strain values around the slip marks is between 2 and 3% and at the large grain (grain 1) close to 1%. This first deformation of the specimen is located in the austenitic phase. These results are in agreement with the one obtained by Le Joncour and coworkers (Joncour et al., 2010) by neutron diffraction. It shows that the domains of elasticity and plasticity of the austenitic and ferritic phases are delimited according to the value of the stress. For applied stress between [200, 600] MPa, it shows that the ferritic phase remains elastic, while the austenitic phase has already plasticized.

At T_22, strains are visible at most of the microstructure components. The strain intensity at the first slip marks increase and are higher than 5%. The strain values at the grain 1 and grain 4 have an average value of 3%. The slip marks, which appear at the grain 4, are linear and parallel to each other. These slip marks could be deformation twinnings, which are originated of the macroscopic work hardening of the material in reference of the results obtained in our previous study in austenitic stainless steel 316 L (Marae Djouda et al., 2018). They occur in the early stage of deformation and present strain intensity in [3 – 4] % bracket. The grain boundary between grains 2 and 3 also presents strain intensity around 3%.

T_1 : Homogeneous strain

T_15 : Very low strain values

Macroscopic behaviour of the material

T_19 : First slip marks

T_22 : Deformation twinnings appearance
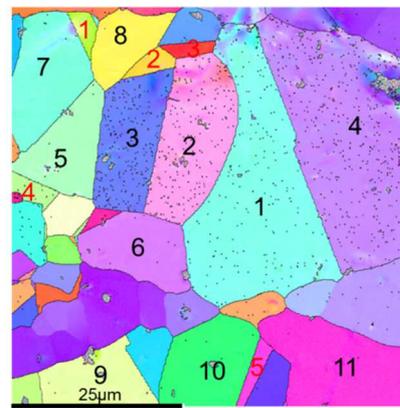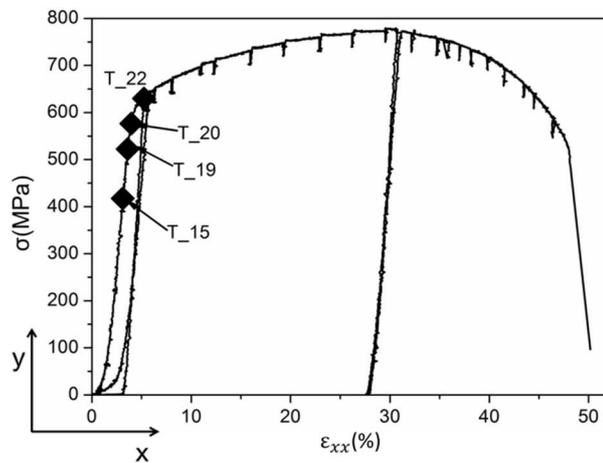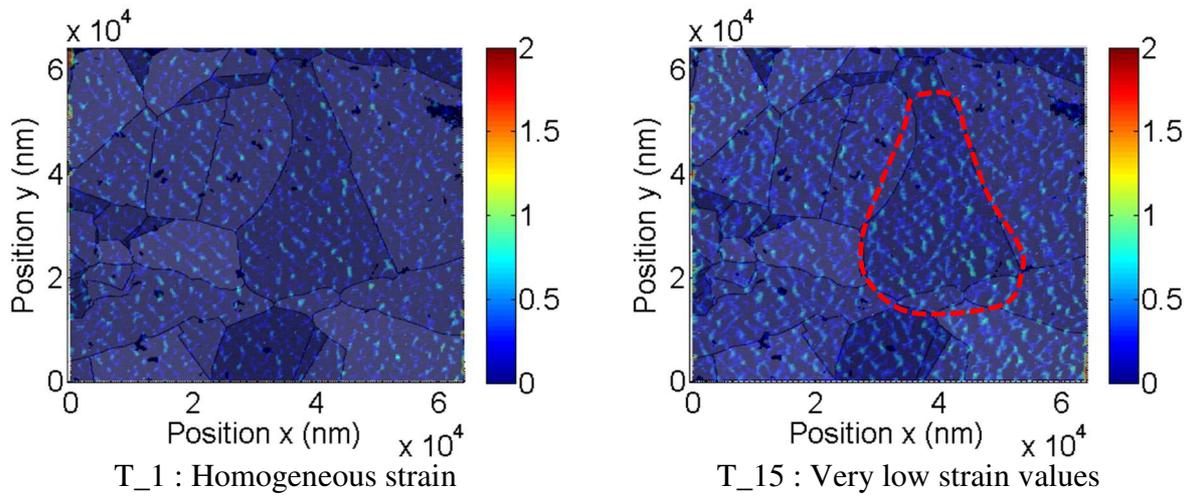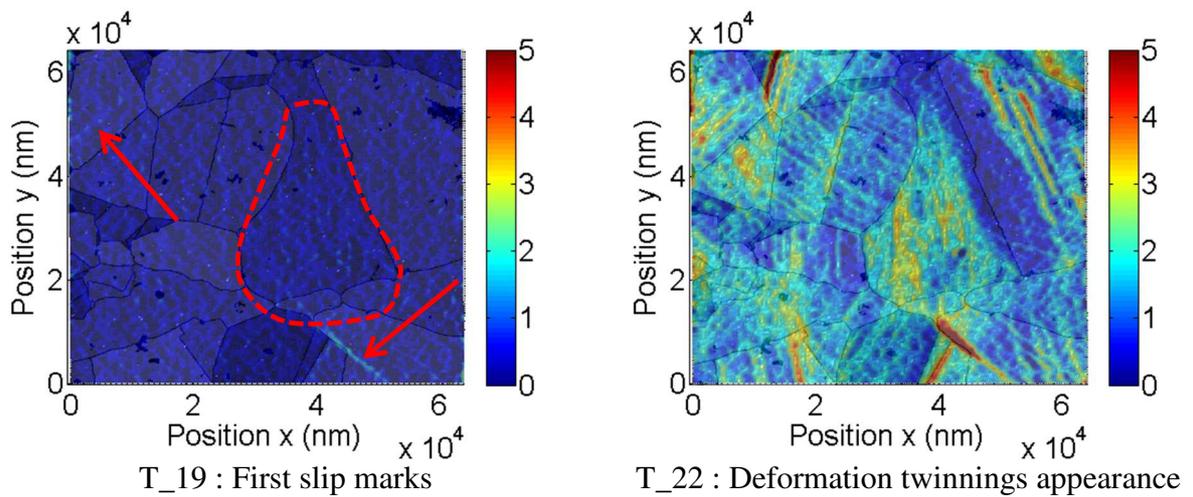
Figure 6: 2D strain maps of Part I of the test.

T_1 : No strain in ferrite

T_15 : No strain in ferrite

Macroscopic behaviour of the material

T_19 : No strain in ferrite

T_22 : Strain initiation in ferrite

Figure 7: Zoom of the strains in the ferritic phase in the Part I

3.1.2. Deformation in the ferritic phase

Ferrite is the hardest phase, so that the deformations are very weak in the first part of the test. The color bar of the strain maps have been reduced and the austenitic phase masked in order to focus only on the evolution in the ferritic microstructure (Figure 7). Before
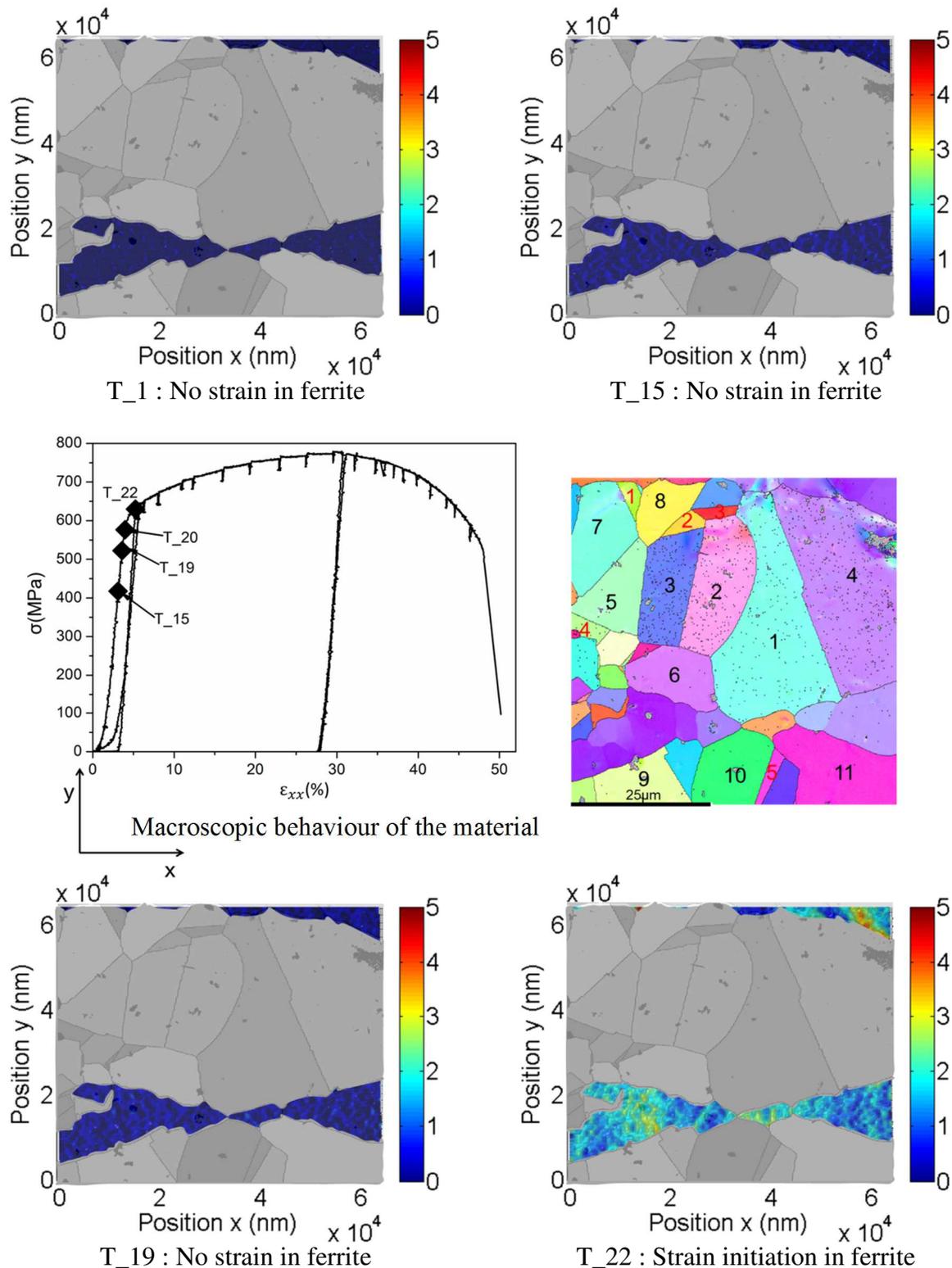
loading level T_22, the ferritic phase presents no visible deformation. At T_22, random distributed strains are visible and have their intensity around 2 and 3%.

In summary, the deformation initiates in the austenitic phase at the vicinity of twins, before the macroscopic elasto-plastic transition. The deformation in the ferritic phase appears after the one of the austenitic phase only at the elasto-plastic transition.

3.2. Analysis of ε_{xx} : Part II of the test

After the second EBSD acquisition, the specimen has been loaded in order to achieve the mechanical conditions obtained at T_22. In this part, local phenomenon of plasticity are analyzed.

3.2.1. Deformations in the austenitic phase

The strain maps for this part of the test are displayed in Figure 8. The population of slip marks especially the one of deformation twinnings increases with the loading. This is shown at the surface of many grains (grains 4, 2 and 8). Their length also increases; for example, in the grain 4, they cross the grain from one boundary to another (along the diameter). The strain intensity at these deformation twinnings is around 15%. The deformation twinnings are indicated in the grains 4 and 8 by consecutive black and red arrows respectively (see Figure 8, T_25).

The increase of the applied load is accompanied by several changes; the width of the deformation twinnings increases until they start to overlap. The maximum strain intensity at the specimen surface is then found at the slip marks. Some slip marks present strain intensity up to 22% (see Figure 8, T_28). The average strain intensity at the surface of some grains is up to 15%; grains 5, 1 and 7. The strain heterogeneities are represented by the fact that at the surface of one grain, there is locally a distribution of strains values (see Figure 8, T_28). The deformation twinnings at the surface of grains 2 and 3 are also visible and are parallel to each another. The contour of many grains are clearly distinguishable.

The strain intensity on the surface of the specimen have increased enough (T_31). At the surface of grain 2, in addition to the previous deformation twinnings, another slip mark appears. This last one is oriented along the larger diameter of the grain. Then two crossing slip systems "cross slips" are activated in the same grain. It probably results to the fact that two different crystallographic plans have been activated in the same grain due to the mechanical solicitation of the specimen. In Figure 8, T_31, the black and red arrows illustrate the primary and secondary slip systems respectively. It also emphasizes the important deformation due to twinning activity of the material. This is visible in the macroscopic behavior of the specimen by the important work hardening. At T_31, the sample have exceeded 25% of the macroscopic deformation and the work hardening is increasing (see the stress-strain curve of the specimen in Figure 8). The strain intensity at some deformation twinnings is up to 30%. Some grains (grains 5, 1 and 7) present average strain intensity up to 25%. The cross slips at the surface of the austenitic phase of duplex stainless steel have been observed by El Bartali et al. during a fatigue test (El Bartali et al., 2008). To achieve this, they correlated the initial EBSD acquisition data with the SEM images of the surface of the sample after fatigue test. In the present study, the strain maps from nanogauges grating evidence the slip marks and cross slip evolution during a tensile test.

When the applied load is continuously increased, strain heterogeneities, strain intensity, and deformation twinning's population and cross slip increase. The slip marks corresponding to the secondary system of the cross slips in the grain 2 also increase.

T_25 : Slips multiplication

T_28 : Strain crack in grain 4

Macroscopic behaviour of the material

Zoom of cross slips in grain 2

T_31 : Cross slips

T_33 : Increased of strain intensity
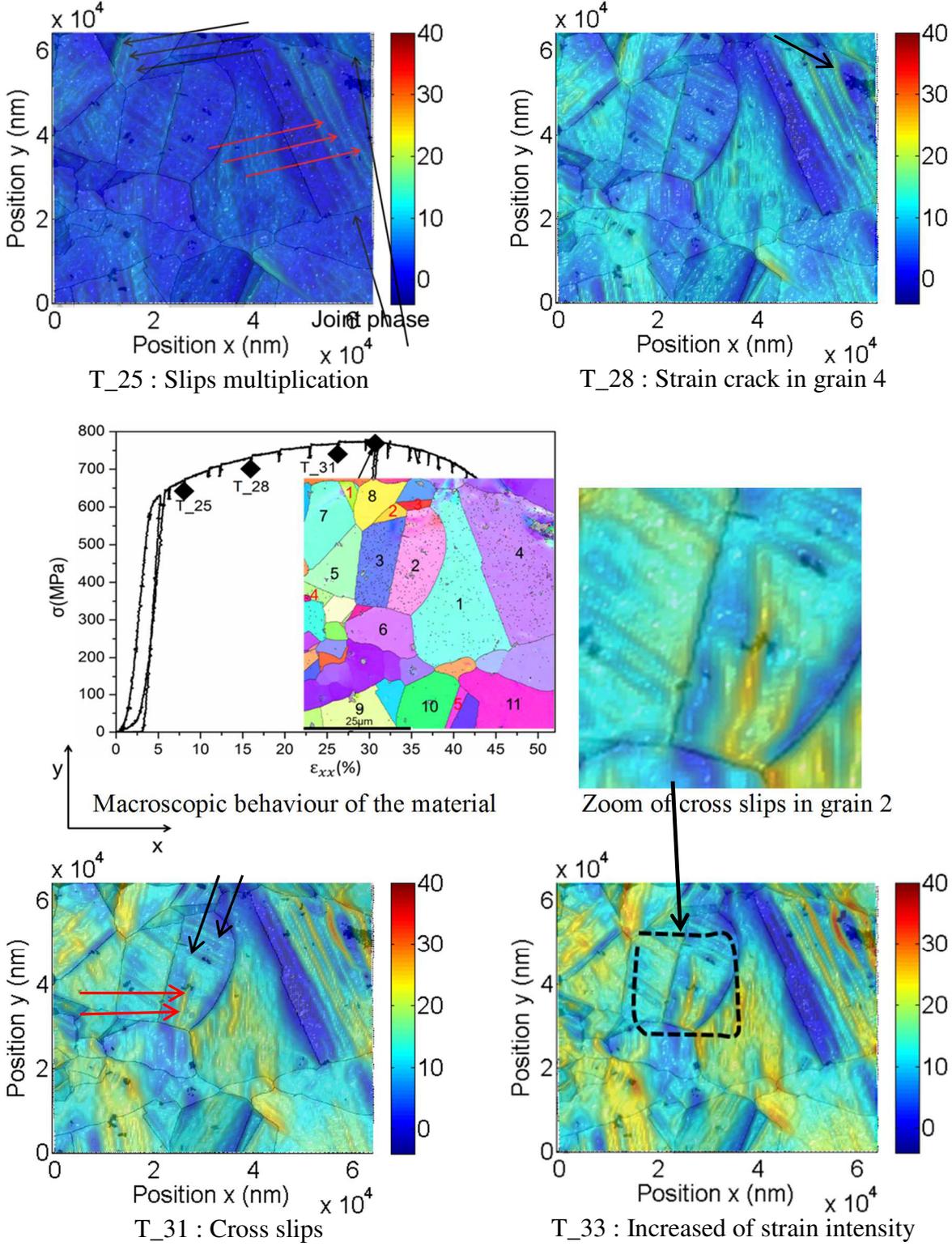
Figure 8: 2D strain maps of Part II of the test. The black arrows in grain 4 show the deformation twinnings (T_25). The black and red arrows in grain 2 show respectively the first and second slip systems activated and form one cross slips system.

T_25 : Deformation of ferrite

T_28 : Slip marks in ferrite

Macroscopic behaviour of the material

Zoom of cross slips in ferrite

T_31 : Another slip marks

T_33 : Increased of strain intensity in ferrite
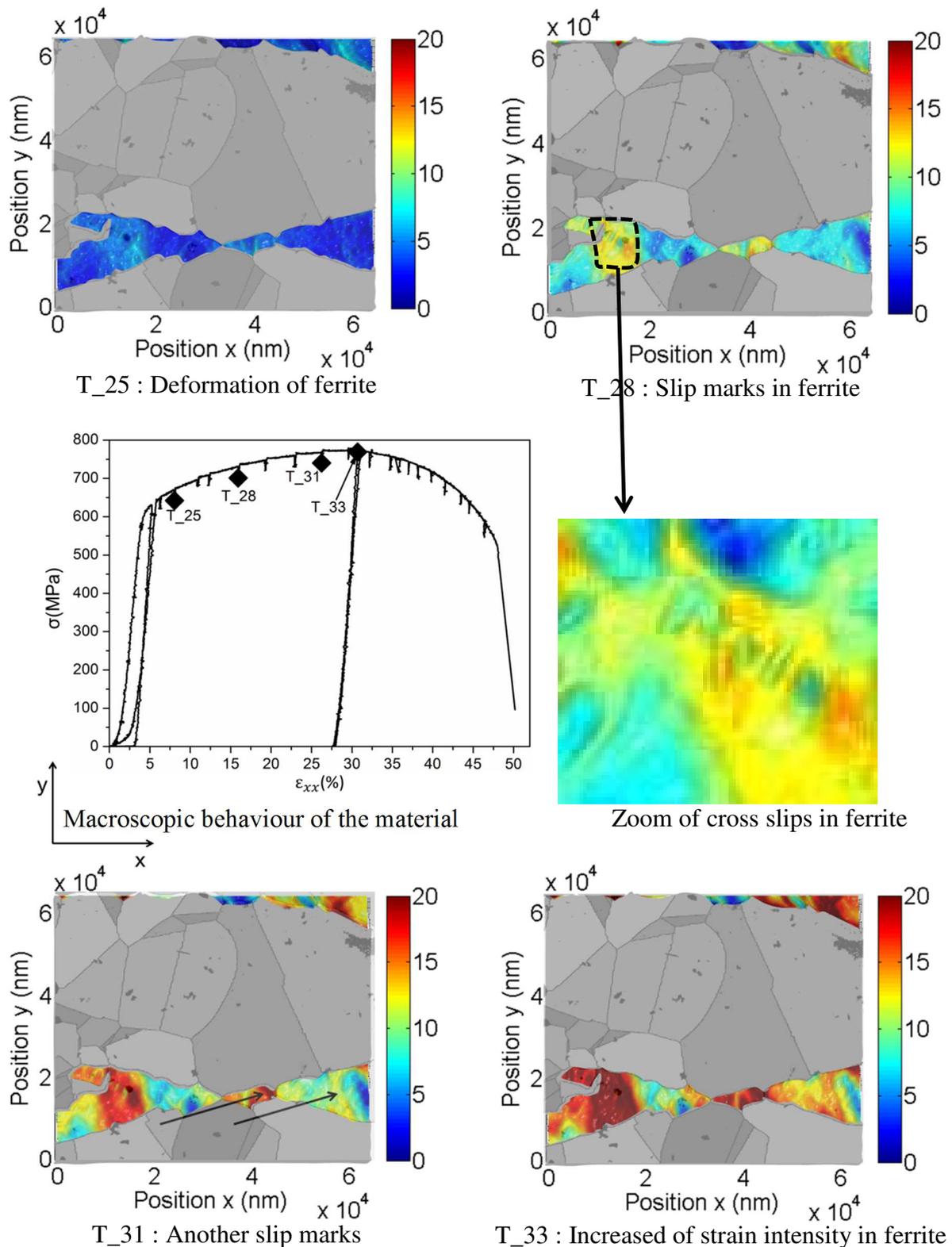
Figure 9: Zoom of the strains in the ferritic phase in the Part II.

3.2.2. **Deformation in the ferritic phase**

The deformation in the ferritic phase begins just at the end of Part I of the test (T_21) with randomly distributed strains. Figure 9 shows the strain evolutions at this phase. The strain intensity reaches values close to 8% at the loading level T_25. At T_28, some slip marks are distinguishable (see the zoom of the T_28 strain map). Because of the geometry of

the slips in the ferritic phase, and the size of the ferrite area in this picture, their analysis is not so easy. They are not straight like the ones observed in austenite, but they are sinuous. Moreover, ferrite presents a cubic centered crystallographic structure, in which the dislocations have three different possible plans for sliding: {110}, {112} and {123}. The sliding directions belong to the <111> family for all the three plans, then the number of the possible sliding system is 48 (more than in austenite). In addition to the fact that the deformations are low (high strength in ferrite), and due to the important number of the possibilities in sliding direction and their geometry, the slip systems are particularly challenging to analyze in the ferritic phase.

Some marks visible at the T_28 loading level are similar to the slip despite their complex geometry. The details from the magnification show that at least two slip systems are activated in this grain.

At T_31, the width of the slip marks increases until they overlap, the strain intensity increases strongly in the ferritic phase. At the previous visible slip marks and in the small grain at the center of the ferritic band, the strain intensity reached 20%. Another's slip marks are visible (indicated by the black arrows in Figure 9, T_31). The strain heterogeneities of the ferritic band are noteworthy.

When the applied loading increases, T_33, the strain intensity increases in the ferritic band, particularly at the slip marks and in the small grain at the middle of the band. The strain heterogeneities become also important. The maximum strain intensity is higher than 20%.

By increasing the loading (T_29), one clearly observes the slips on the grain of the right part of the grating. The deformations on the left side and the joint of phase on the upper right part reach 20%. At T_33, the deformations increase more: they exceed 20% on the left part, on the small grain in the center of the ferritic band and on the upper right part of the grating. The deformation is 15% at the grain of the right part of the ferritic band. Beyond the loading level of T_29, ferrite plasticizes strongly, the values of the deformation increase rapidly: from 15% to T_28 to more than 20% to T_33. The cross-slip system on the surface of grain 2 is visible at level T_29. It is also around this level of loading that a strong plasticization of ferrite is now registered. In the first part of the test, there has been also a rapid multiplication of slips on the surface of austenite grains, as well as the appearance of the first deformations in ferrite. We can then say that the increase of the deformation in ferrite is accompanied by a strong deformation imposed in austenite. This could be justified by the difference in hardness of the two phases, which implies a greater deformation in austenite, for the same level of constraint imposed.

3.3. Analysis of ε_{xx} : Part III of the test

In Part III of the test, the strain heterogeneities have grown in such a way that the grain contours are no longer distinguishable. Moreover, deformation pass from one grain to another through the boundaries and slips. Figure 10 shows the strain map of the T_36 loading level belonging to the part III. It becomes difficult to distinguish the austenitic and ferritic phases because the strain intensities at the ferritic phase have also strongly increased. The strain intensity at certain slip marks is up to 40%, at certain grains up to 30%.

In summary, the local strain evolution at the microstructure components of the two phases is different. The deformations are initiated in the austenitic phase at the vicinities of

twins and the specimen still in the elastic domain when the first marks are visible. The first deformation marks in the ferritic phase appear at the elasto-plastic transition. When the specimen is stressed, the elastic limit of the austenitic phase is reached first, it is around 420 MPa. Locally, the first marks of the deformations are visible there. The first deformation marks in the harder ferritic phase appear when the material enters in plasticity at the macroscopic level. The appearance of deformation marks in the ferritic phase is locally accompanied by a multiplication of the deformation twinning population. This implies that for a stress applied to the material, the deformation is greater in austenite, which is more ductile than ferrite. This is clear when comparing images T_22 in Figures 7 and 8. It can also be said that the deformations of ferrite impose greater deformation in austenite. For example, at the stress level T_29, the deformations in the ferritic phase become important, at the same time cross-deformations are visible in austenite, corresponding to a balance of the loading.
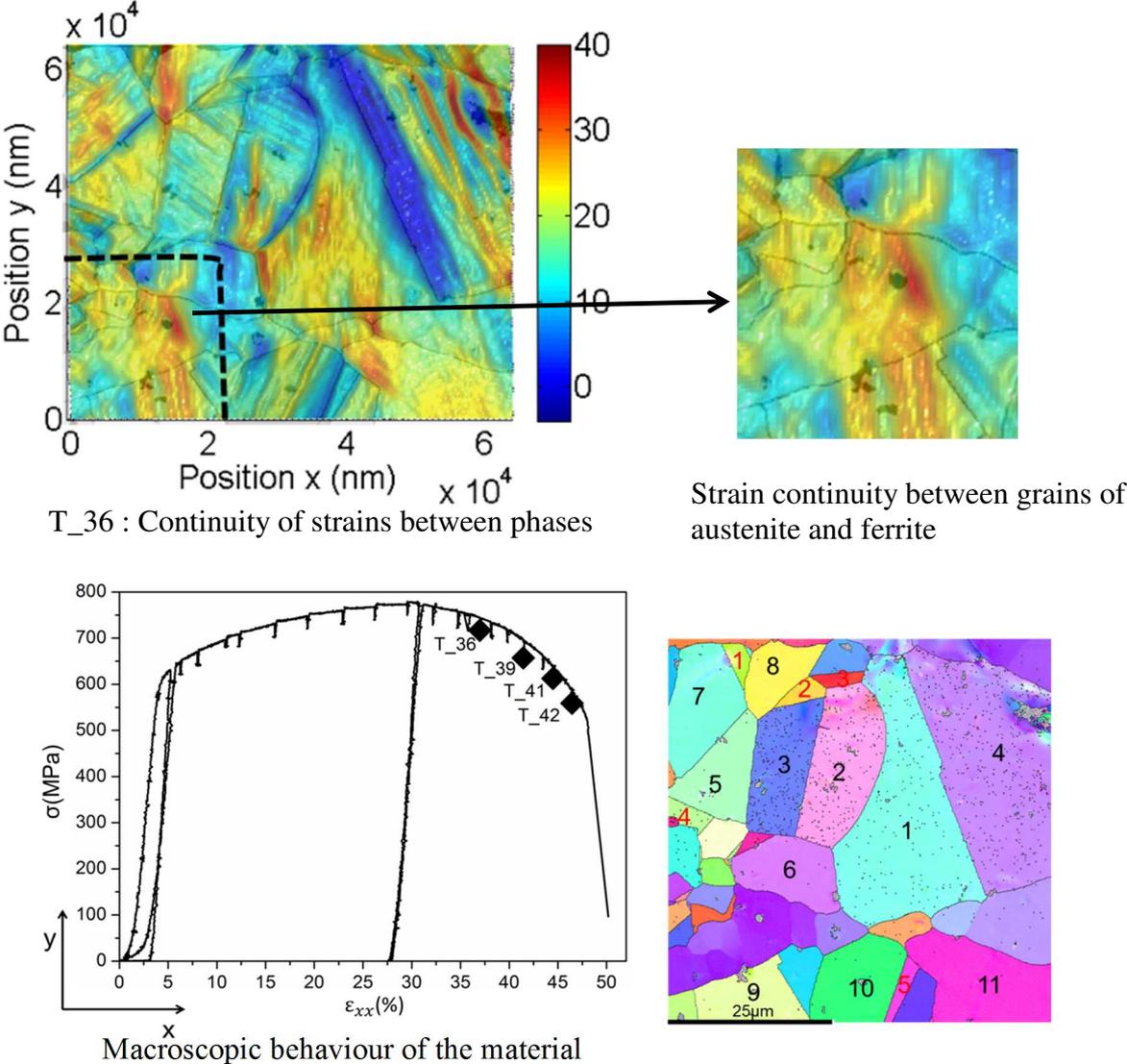

T_36 : Continuity of strains between phases

Strain continuity between grains of austenite and ferrite

Macroscopic behaviour of the material

Figure 10: 2D strain maps of Part III of the test.

4. Distortion analysis

The use of NPs as nanogauges allows following the strain distribution within the microstructure components in relation to the macroscopic behavior of the specimen. In addition to the strain maps obtained from the components of the Euler-Almansi tensor, other kinematic fields can provide interesting information about the behavior of materials and have been investigated. For example, to highlight local disorientations on a part of a grain or at the grain boundary, the distortion maps can be analyzed. The distortion is defined as a local angle variation between 4 NPs. Details can be found in (Marae Djouda et al., 2018).

Figure 11 shows some distortion maps corresponding to the three parts of the test. At the loading level T_2, the distortion values are almost null. This is entirely consistent since the reorientations of the crystallites are not initiated within the microstructure. When the applied load increases, the NP displacements are visible locally for specific components: at twins vicinities, at some grain boundaries and at the surface of large grains (see Figure 11, T_22). The distortion marks at the grain 4 illustrates the first deformation twinning, which appears on this grain. The boundary between grains 2 and 3 is also visible. All these marks have been visible in the strain maps for the corresponding loading level.

Another deformation twinnings appear at the surface of grain 4 with the mechanical solicitation (T_28). The corresponding marks are parallel to each other and the value of distortion is -0.2. In the grains 2 and 3, the deformation twinnings are also visible at their surface. The heterogeneities of deformations are also highlighted in the distortion maps by the local variations in the values. The ferritic phase is distinguishable because of its almost null distortion values (see Figure 11, T_28).

At T_36, with the applied load, some distortions are visible in the ferritic phase especially around the boundary phase close to Grain 9 (see Figure 11, T_36). The rest of the grating surface reflects the local heterogeneities of deformation. For example, Grain 1 presents very marked heterogeneities of deformations; the lower part of this grain presents negative distortion values and the upper part have its distortion around zero. The boundary phase close to Grain 4 presents an important distortion intensity (around 0.4), it probably corresponds to a strain barrier where the slip marks concentrate their deformation. Some grains present important distortion intensity like grains 2, 3, 5 and 11.
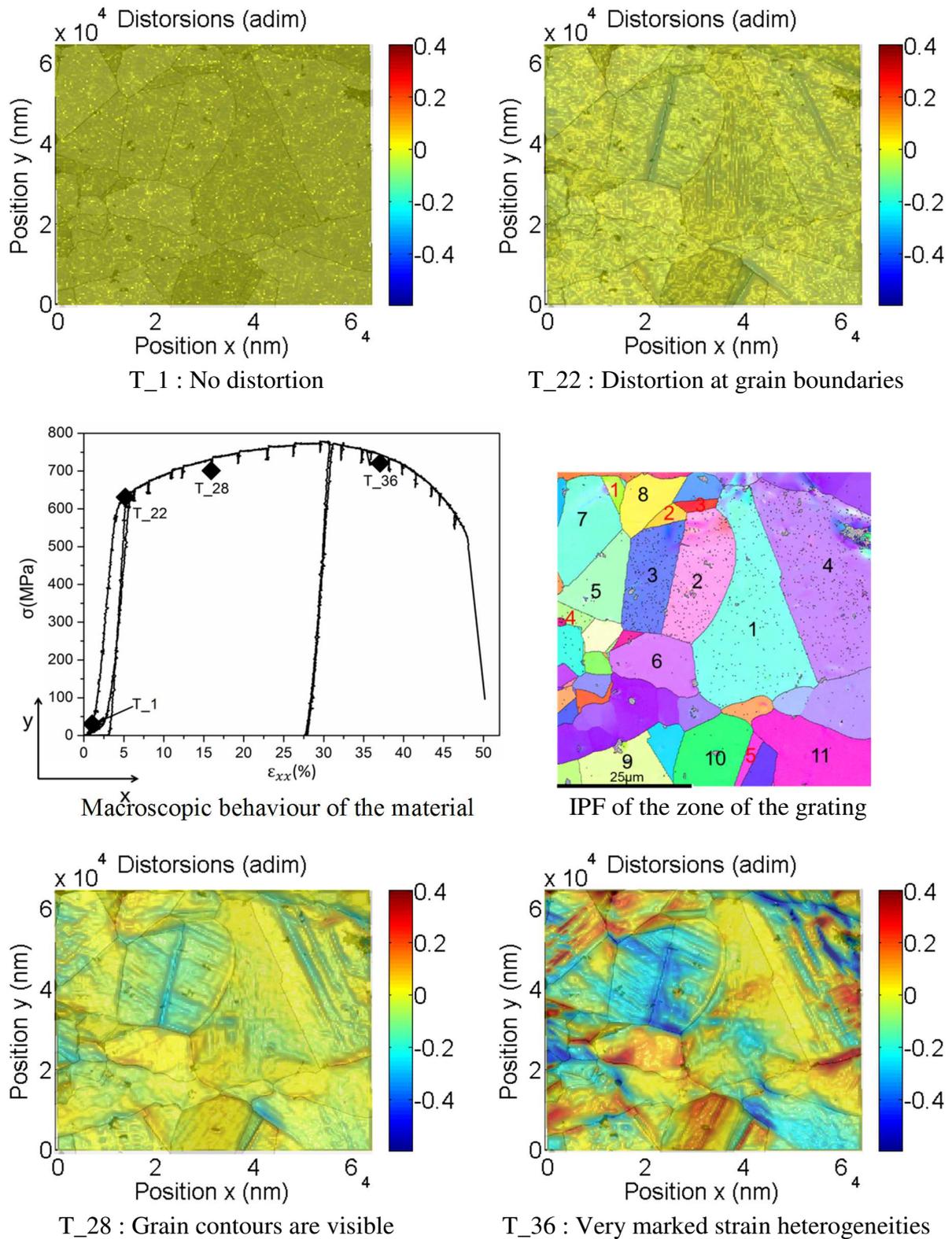
Figure 11: 2D distortion maps, maps T_2 and T_22 belong to the first part of the test. At T_2, the distortion value is almost null because there is any visible deformation activity at the specimen surface. The deformation mechanism, which are visible in strain maps are highlighted in distortion at T_22 level. T_28 and T_36 belong to the part II and part III respectively, they show an increase of strain heterogeneities with the mechanical applied loading.

5. EBSD analysis and comparison with kinematic fields

The analysis of the deformation fields obtained from NP displacements correlates local kinematic fields with the macroscopic behavior of the specimen. To go further in the analysis of the local deformation mechanisms, the crystallographic data of the analyzed zone can also bring important information. The EBSD technique (Dingley and Randle, 1992; Field, 1997) have been used to perform three crystallographic acquisitions of the interest zone at three different steps of the test: before traction (T_0), at loading level T_22 (elasto-plastic transition) and at loading level T_33 (plasticity). To perform EBSD acquisition at loading levels T_22 and T_33, the traction has been stopped and the applied force on the sample has been discharged until zero.

5.1. Inverse pole figures

Inverse pole figures (IPF) are used to locally evaluate crystallographic orientations using a color code. They show the orientation of an axis of the sample in the reference of the crystal. The crystallographic orientations in each phase of the grating area for the three EBSD acquisitions have been studied.

5.1.1. Austenitic phase

Figure 12 shows the IPFs of the grating zone for the three EBSD acquisitions. In these figures, the ferritic phase has been removed in order to focus on the evolutions of the austenitic phase in the first time. The black points correspond to the non-indexed zone of the surface of the sample, and their population progressively increases in the figures of the plastic domain. This is because the specimen surface becomes rough. It affects the EBSD acquisition quality and also leads to NPs deformation. NP positioned at the slip mark can experience severe deformation. This deformation results to the change of the NPs shape and then lead to errors in strain quantification (Marae Djouda et al., 2018). The IPFs show that grains exhibit crystallographic orientations different from the ones of the neighboring grains. This diversity in the orientations can be explained by a good recrystallization during the thermal treatment that has been applied to the material (Badji et al., 2011). The IPF at the initial stage presents no texture. Similar observations have been observed in previous works on the same type of duplex material (Wroński et al., 2012). The grains are also heterogeneous in size: the diameter varies between tens and hundreds of microns.

The comparison between the first EBSD acquisition (initial state) (Figure 12a) and the second one (Figure 12b) shows that the crystallographic orientations have locally changed at some grains. These crystallographic variations are shown by the color changes. The grains on which the variations are significant are the grains 1, 4, 8 and 5. The grains 1 and 4 are the two largest grains of the zone of the grating. These color variations reflect the dislocation activity in the volume of the material. These observations are consistent with the strain maps obtained in the first part of the test (see Figure 6). Indeed, after the initiation of the deformation at the vicinities of some twins, slip marks have been found at the surface of many grains in the austenitic phase. The crystallographic information corroborate the kinematic results presented in the previous sections concerning the first part of the test. Although the EBSD gives details on the nature of the microstructure components and the crystallographic changes due to the deformation and rotation, it presents lacks in the description of the mechanism of the deformation. For example, deformation twinnings cannot be distinguished.

The change in the local orientations in the plastic domain are noticeable in comparison to the IPF at the initial state and at the end of Part I. The heterogeneities of deformation are clearly visible. The grains surface, which has initially a preferential crystallographic orientation, present locally different crystallographic orientations (see Figure 12c). These heterogeneities have been quantified in the strain and distortion maps. For example, the upper part of the grain 1 has its orientation (between <101> and <111>) different from the lower one (<101>). The important heterogeneity is due to the elongation and rotation of the microstructure components in order to accommodate the applied loads. The necking of austenite band study herein is visible (see Figures 12a and 12c). The slip marks at the surface of certain grains are clearly visible; they are indicated by arrows in the Figure 12c. They have a specific crystallographic orientation compare to the parent grains. These slip marks correspond to an overlap of deformation twinnings. These marks are globally located on the surface of the grains having in their immediate vicinity a twin.

Figure 12: Inverse pole figure maps a) at the initial state, b) at the elasto-plastic transition (EBSD_0), and c) in the plastic domain (EBSD_1) in the austenitic phase. The numbers are assigned to grains (in black, 1 to 11) and twins (in red, 1 to 5).

5.1.2. **Ferritic phase**

In the ferritic phase, in opposite to the austenitic phase, the grains are larger and have very similar orientations between <001> and <111> (see Figure 13). This is justified by the

partial recrystallization of crystallites in this phase (Wroński et al., 2012). At the loading level T_22, the changes in color are not very important and correspond to a very low activity of the dislocations. The kinematic maps show that, at this loading level, the ferritic phase just initiates its plasticity (see Figure 7, T_22). The ferritic phase harder than the austenitic phase comes into plasticity long time after the austenitic phase has plasticized. The IPF at the end of the part II of the test (see Figure 13c) shows noticeable variation in colors. It indicates that at this stage of the test, the deformation of the ferritic phase is effective. Some slip marks are also visible, but they are less distinguishable compare to the ones in austenitic phase. Moreover, their width is more important. These observations are in concordance with the evolution observed in strain maps. It confirms that the marks in these lasts are effectively slip marks.
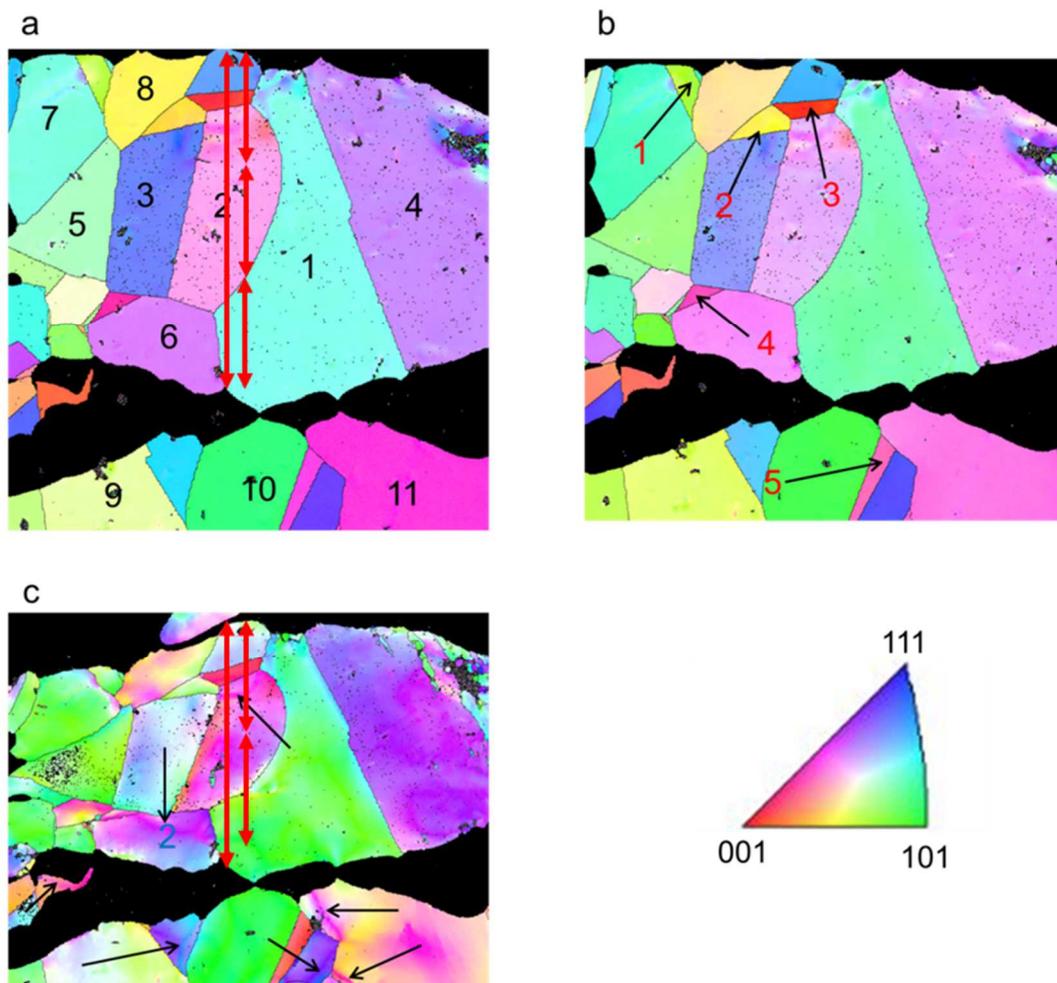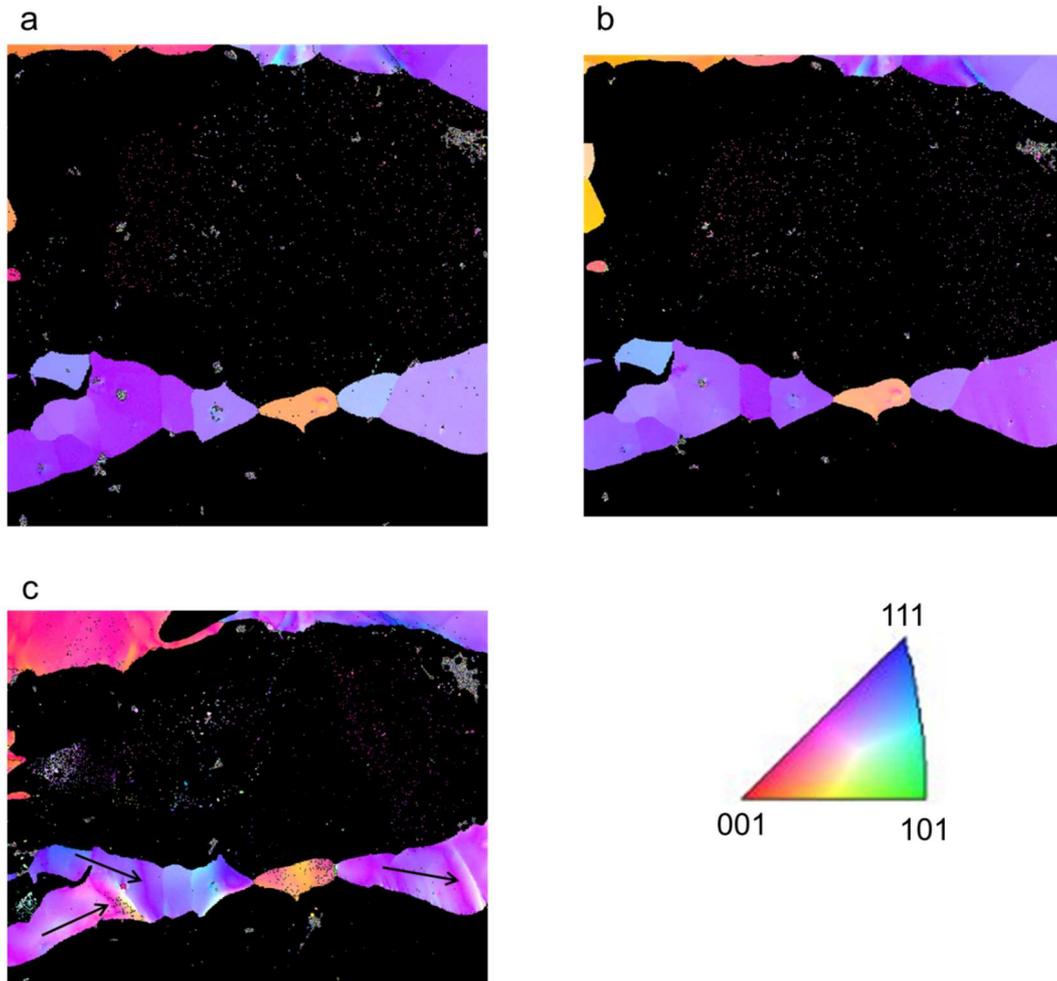
Figure 13: Inverse pole figure maps a) at the initial state, b) at the elasto-plastic transition (EBSD_0), and c) in the plastic domain (EBSD_1) in the ferritic phase.

5.2. Disorientation

Disorientation can be used to quantify locally the strain at the grain level (Quey et al., 2015, 2012; Wroński et al., 2012). Indeed disorientation evaluates the angle variation between two crystallites created by the application of the mechanical loading. During the deformation, atoms move from their equilibrium position and then create modifications in the crystal structure. The disorientation is a relevant parameter thus making it possible to account the relative displacements of the crystallites of the material. Indeed when one crystal change position in the matter, one angle can be defined with another reference crystal. Assuming that the surface of the specimen is perfectly flat, it has been shown that the error in disorientation is 0.2° and increases with the differences between crystallographic planes in grain caused by the deformations. The error is therefore greater for the acquisition EBSD_2, which has been carried out after plastic loading of the specimen.

5.2.1. Austenitic phase

The disorientations are grouped into three intervals: [0 ° - 3°], [30 ° - 60 °] and 60 ° and more (see Figure 14). The evolutions are shown for the three EBSD acquisitions realized at three different loading levels. At the initial stage, the three groups present a quite proportional population of disorientations. This distribution is different from the one obtained

in an austenitic stainless steel (single phase steel) where the distribution of disorientations has been almost uniform at the Part I of the test (Marae Djouda et al., 2018). The slight difference may be related to the nature of the material (two phases in presence) and / or to the thermo-mechanical treatment.

At the EBSD_1, the global change in disorientation is not considerable compared to the one obtained in the case of an austenitic stainless steel. In the specimen studied herein, a slight decrease in the proportion of the crystallites disoriented between [0° - 3°] bracket and 60° and more is observed. In the corresponding strain map, some slip marks are visible. It then appears that the slip activity in the volume of the material does not cause at this stage any significant variations in the disorientation in comparison with the case of austenitic stainless steel 316L. It appears that the presence of the ferritic phase in the duplex steel modify greatly the deformation of the austenitic phase. The thermo-mechanical treatment of the duplex steel could also play an important role.

The variations in the EBSD_2 acquisition are more pronounced. The crystallites disoriented in [0° - 3°] bracket increase and represent more than the half of the proportion of the crystallites population in the grating zone. This results is different from the one obtained in the austenitic stainless steel 316L (Marae Djouda et al., 2018) where in the plastic domain the crystallites where mainly [30° - 60°] bracket disoriented and their proportion close to 0.7. It means that the local mechanism of the deformation are not exactly the same. The presence of the ferritic phase with a higher strength rules the deformation of the austenitic by imposing some incompatibilities of deformations. However, the trends observed in the crystallite population evolutions at the elasto-plastic transition have the same evolution that the one for pure austenitic phase, but with different proportions. This could underline a possible competition between mechanisms of deformation in the pure austenite and the incompatibilities of deformations imposed by the ferritic phase. Moreover, when increasing the mechanical stress, mechanisms in the ferritic phase emerge.
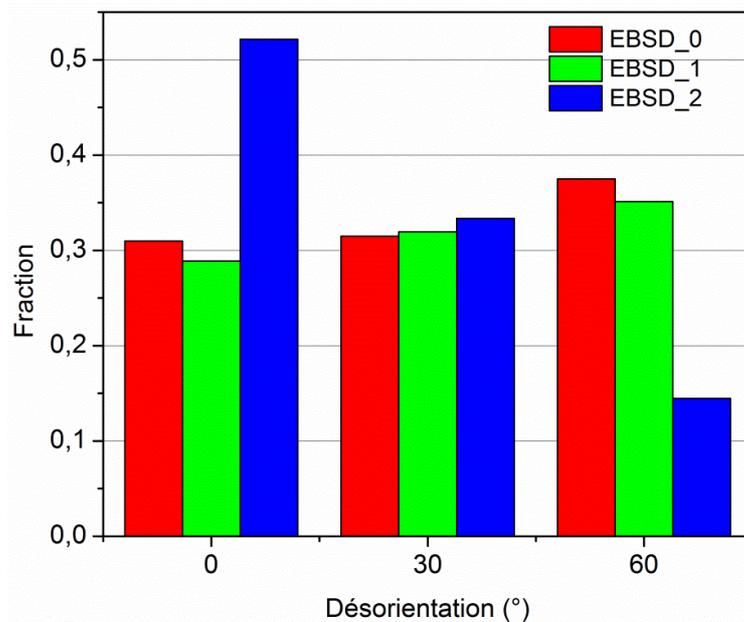

Figure 14: Evolution of the disorientation angle in austenitic phase.

5.2.2. **Ferritic phase**

At the initial stage (EBSD_0), the crystallites are distributed as a function of the intervals; 0.23 for [0° - 3°] bracket, [30° - 60°] bracket and 60° and more present close proportions, 0.39 and 0.38 respectively (see Figure 15). In the two others EBSD, the population of the crystallites disoriented between 60° and more decreased and reached 0.18 at the EBSD_2. At the same time, the crystallites disoriented between [0° - 3°] bracket and [30° - 60°] increased progressively. This last interval concerns the half of the population of the crystallites. It is important to note that the population of the crystallites disoriented between [0° - 3°] bracket increases with the loading in both the austenitic and the ferritic phases. It has been observed for the loading level up to T_30, a propagation of slips between the two phases (see Figure 10). The crystallites presenting the same disorientation in both phases could facilitate the propagation of the deformation between phases. The incompatibilities of deformations are then broken. The relations of orientation between the two phases can be explained by the Kurdjumov - Sachs (K-S) relations (Godet et al., 2004; Wittridge et al., 2001). They are expressed in the following way: $\left(111\right)\left\langle1\bar{1}1\right\rangle_{\delta}\left(110\right)\left\langle1\bar{1}1\right\rangle_{\gamma}$ which shows that the two phases have a common dense plane. A dense direction is associated to each of the planes, therefore common sliding systems between phases.
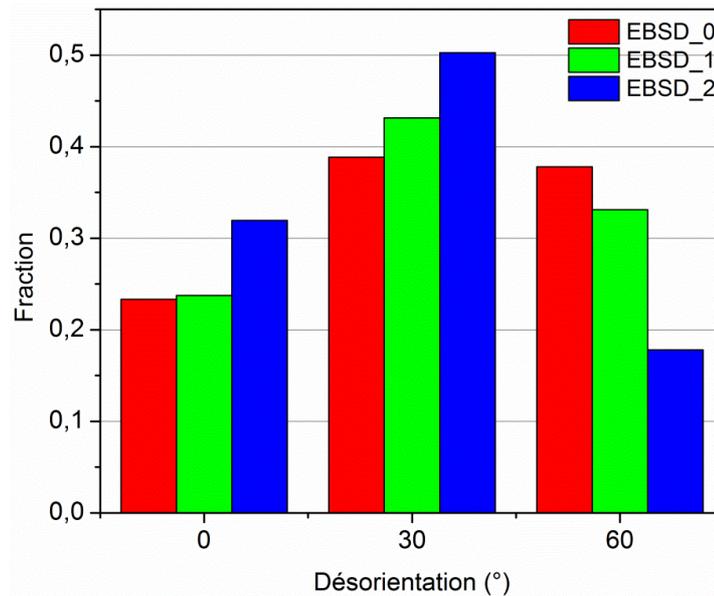
Figure 15: Evolution of the disorientation angle in ferritic phase.

6. **Discussion of the results**

Metal NPs used as nanogauges allow a quantitative investigation of strains mechanisms at the local scale. Coupled with EBSD acquisition, the deformation of the microstructure components can be quantified. The evolution of kinematic fields at the surface of a duplex steel UR45N has been analyzed in the present study. It appears that plastic phenomena arise at specific moments of the macroscopic evolution and affect the microstructure in specific way. The strains evolutions in austenitic and ferritic phases are different and influence each other. The austenitic phase, which is less strength, enters in plasticity first and the strain marks at it surface are visible primarily near the twins. These evolutions become visible before the elasto-plastic transition in comparison to the

macroscopic behavior of the specimen. One can also notice that compare to pure 316L stainless steel (Marae Djouda et al., 2018), in the duplex steel UR45N the clues showing austenite enters in plasticity appear later. This probably illustrates the interactions between the two phases in presence, when the material is undergoing external mechanical loadings. Ferrite only showplasticity evidence at the elasto-plastic transition and the strains on its surface are very heterogeneous. The beginning of plasticity in ferrite is accompanied with the increase of slip marks population in austenite and specifically deformation twinnings. These observations have been confirmed by the crystallographic EBSD analysis at the elasto-plastic transition. The inverse pole figure at the elasto-plastic transition showed several changes in some grains of austenite. These are the largest grains. However, the changes in ferrite are very weak and are in agreement with the strain maps, which present a very weak strain intensity.

When the applied load increases, the local strain maps show a global increase of the strain intensity. The slip marks and the deformation twinning's population increase simultaneously and their strain intensity also increases. In the austenitic phase, the slip marks are first limited around the grain boundaries in which they are located. For the austenitic grains at the frontier with ferrite, the phase boundaries react as strain barriers: the deformation of the slips concentrated at their vicinities. This is visible at the strain maps in the tensile and transverse directions (see supplementary materials). The augmentation of the applied load is accompanied by an increase of the strain intensity of the phase boundaries (barriers), until the moment when the barrier failed. Once the barrier has failed, the deformation can go through one phase to another with respect to the incompatibilities of deformations. The slip marks at the top of ferrite are sinuous in geometry and appear in plastic domain. When they are visible, some cross slips appear progressively in austenite. It proves that in combination with the twinning activity, the mechanical work hardening in austenite is significant and constitutes the more important part of the work hardening of the material. Some slip marks are visible in the inverse pole figure of the plastic domain both in austenite and in ferrite.

It also appears that the deformation mechanisms of austenite in the presence of ferrite is different from the ones in the pure austenitic phase (316L). This is highlighted in the crystallographic analysis. The disorientation can be related to the strain intensity in the volume of the material. The disorientation of the crystallites have been classified in three different groups: [0° - 3°], [30° - 60°] brackets and 60° and more. The evolution of the disorientation populations in the three groups shows that the presence of the ferritic phase rules the deformation of the austenitic by imposing some incompatibilities of deformations. A possible competition between mechanisms of deformation of the pure austenite and the incompatibilities of deformations imposed by the ferritic phase could also happened.

The strain maps also illustrate the very pronounced heterogeneities of the material surface. Indeed, in a same grain, several strain intensities are visible. The importance of the combination of austenite and ferrite phases appear clearly by the mechanism of their local deformation and their interactions. Austenite bring an important work hardening via the slips and the twinning activity. Ferrite with a higher hardness increases the elastic limit and the ultimate tensile strength of the material.

7. Conclusions

The duplex alloy UR45N has been analyzed by coupling a strain measurement method based with the use of a gold NPs grating with the EBSD technique during an in-situ tensile test. The evolution of some of the kinematic fields in each phase have then been highlighted. The SEM images and strain maps allow a quantitative analysis of the deformation initiation at each of the material phase. Indeed, the austenitic phase enters first in plasticity; the strains are initiated at the vicinity of the twins and are followed by the appearance of slip marks at the surface of some grains when the applied load increases. At the same time, in the ferritic phase, the plastic marks appear only at the elasto-plastic transition. Once the ferritic phase enters in plasticity, the population of the slip marks in the austenitic phase increases greatly.

The population of the slip marks in the austenitic phase increases progressively with the applied load in the second part of the test. Some of these slip marks are deformation twinnings and are parallel to each other. Their population in the same grain and the strain intensity is also function of the applied loading. The slip length is first limited inside the grains by grain boundaries and phase boundaries. These last react as barrier of strains, such that strain concentrations are visible at their location. The strains in the ferritic phase are first randomly distributed. Then slips are visible at the surface, they are sinuous and larger in width compared to the ones in austenite; they get entangle each other. The slip and twinning activities in the austenitic phase mainly contribute to the mechanical work hardening of the material. The elongations and rotations of the austenitic microstructure components accompany the plasticity. Combined with the slip and twinning activities, these result in the heterogeneity of deformations. The mechanical work hardening of the specimen increases; the cross slip systems appear at the surface of the austenitic phase. These cross slips have been recorded also at the surface of austenitic stainless steel 316L.

However, the local mechanisms of deformation austenitic phase in the pure austenitic steel and the one from duplex steel are different. In the case of pure austenitic steels, most of the crystallites are disoriented in [30° - 60°] bracket, while in the present duplex steel, they are distributed in [0° - 3°] bracket. In the ferritic phase, crystallites are disoriented in the plastic domain between [0° - 3°] and [30° - 60°] brackets. The most important population is disoriented in [30° - 60°] bracket. At the third part of the test, strains propagate between phases. It seems to be allowed by the crystallites, which present the same disorientation in both phases: [0° - 3°] bracket.

The kinematic fields' maps highlight the phenomena of plasticity at the microstructure components of each phase and their interactions. The NPs used like nanogauges allow a fine analysis of the evolutions of strains at the phases and theirs interactions. The kinematic fields also give the strain quantification during an in-situ tensile test. This original study in which the nanogauges grating and EBSD technic are complementary used bring a deep comprehension of the deformation of the duplex steel UR45N. It also allows a good comprehension of the local mechanisms of the deformation of each phase and the pertinence of combining two phases.

References

Aubin, V., 2006. Plasticité cyclique d'un acier inoxydable austéno-ferritique sous chargement biaxial non-proportionnel. U niversité des Sciences et Technologie de Lille.

Badji, R., Bacroix, B., Bouabdallah, M., 2011. Texture, microstructure and anisotropic properties in annealed 2205 duplex stainless steel welds. Mater. Charact. 62, 833–843. https://doi.org/10.1016/j.matchar.2011.06.001

Bugat, S., 2000. Comportement et endommagement des aciers austeno-ferritiques vieillis : une approche micromécanique. Ecole Nationale Supérieure des Mines de Paris.

Clair, A., Foucault, M., Calonne, O., Lacroute, Y., Markey, L., Salazar, M., Vignal, V., Finot, E., 2011. Strain mapping near a triple junction in strained Ni-based alloy using EBSD and biaxial nanogauges. Acta Mater. 59, 3116–3123. https://doi.org/10.1016/j.actamat.2011.01.051

Dingley, D.J., Randle, V., 1992. Microtexture Determination by Electron Back-Scatter Diffraction. J. Mater. Sci. 27, 4545–4566. https://doi.org/Doi 10.1007/Bf01165988

El Bartali, A., Aubin, V., Sabatier, L., Villechaise, P., Degallaix-Moreuil, S., 2008. Identification and analysis of slip systems activated during low-cycle fatigue in a duplex stainless steel. Scr. Mater. 59, 1231–1234. https://doi.org/10.1016/j.scriptamat.2008.07.044

Field, D.P., 1997. Recent advances in the application of orientation imaging. Ultramicroscopy 67, 1–9. https://doi.org/10.1016/S0304-3991(96)00104-0

Fréchard, S., Martin, F., Clément, C., Cousty, J., 2006. AFM and EBSD combined studies of plastic deformation in a duplex stainless steel. Mater. Sci. Eng. A 418, 312–319. https://doi.org/10.1016/j.msea.2005.11.047

Godet, S., Glez, J.C., He, Y., Jonas, J.J., Jacques, P.J., 2004. Grain-scale characterization of transformation textures. J. Appl. Crystallogr. 37, 417–425. https://doi.org/10.1107/S0021889804007320

Hariharan, K., Majidi, O., Kim, C., Lee, M.G., Barlat, F., 2013. Stress relaxation and its effect on tensile deformation of steels. Mater. Des. 52, 284–288. https://doi.org/10.1016/j.matdes.2013.05.088

Jia, N., Peng, R.L.I.N., Brown, D.W., Clausen, B., Wang, Y.D., 2008. Tensile Deformation Behavior of Duplex Stainless Steel Studied by In-Situ Time-of-Flight Neutron Diffraction. Metall. Mater. Trans. A 39A. https://doi.org/10.1007/s11661-008-9675-2

Joncour, L. Le, Panicaud, B., Baczman, A., Francois, M., Braham, C., Paradowska, A., Wron, S., Chiron, R., 2010. Mechanics of Materials Damage in duplex steels studied at mesoscopic and macroscopic scales. Mech. Mater. 42, 1048–1063. https://doi.org/10.1016/j.mechmat.2010.10.003

Marae Djouda, J., Madi, Y., Gaslain, F., Beal, J., Crépin, J., Montay, G., Le Joncour, L., Recho, N., Panicaud, B., Maurer, T., 2018. Investigation of Nanoscale Strains at the Austenitic stainless steel 316L surface : Coupling between Nanogauges Gratings and EBSD Technique during in situ Tensile Test . Mater. Sci. Eng. A 740–741, 316. https://doi.org/10.1016/j.msea.2018.10.059

Marae Djouda, J., Montay, G., Panicaud, B., Béal, J., Madi, Y., Maurer, T., 2017.

Nanogauges gratings for strain determination at nanoscale. Mech. Mater. 114, 268–278. https://doi.org/10.1016/j.mechmat.2017.08.014

Maurer, T., Marae-Djouda, J., Cataldi, U., Gontier, A., Montay, G., Madi, Y., Panicaud, B., Macias, D., Adam, P.M., Lévêque, G., Bürgi, T., Caputo, R., 2015. The beginnings of plasmomechanics: towards plasmonic strain sensors. Front. Mater. Sci. 9, 170–177. https://doi.org/10.1007/s11706-015-0290-z

Morgeneyer, T.F., Taillandier-Thomas, T., Helfen, L., Baumbach, T., Sinclair, I., Roux, S., Hild, F., 2014. In situ 3-D observation of early strain localization during failure of thin Al alloy (2198) sheet. Acta Mater. 69, 78–91. https://doi.org/10.1016/j.actamat.2014.01.033

Quey, R., Dawson, P.R., Driver, J.H., 2012. Grain orientation fragmentation in hot-deformed aluminium: Experiment and simulation. J. Mech. Phys. Solids 60, 509–524. https://doi.org/10.1016/j.jmps.2011.11.005

Quey, R., Driver, J.H., Dawson, P.R., 2015. Intra-grain orientation distributions in hot-deformed aluminium: Orientation dependence and relation to deformation mechanisms. J. Mech. Phys. Solids 84, 506–527. https://doi.org/10.1016/j.jmps.2015.07.014

Wittridge, N.J., Jonas, J.J., Root, J.H., 2001. A Dislocation-Based Model for Variant Selection during the gamma-to-alpha prime Transformation. Metall. Mater. Trans. A 32A, 889–901. https://doi.org/10.1007/s11661-001-0346-9

Wroński, S., Tarasiuk, J., Bacroix, B., Baczmański, a., Braham, C., 2012. Investigation of plastic deformation heterogeneities in duplex steel by EBSD. Mater. Charact. 73, 52–60. https://doi.org/10.1016/j.matchar.2012.07.016

Zhao, Y., Gadali, E., Braham, C., Panicaud, B., François, M., Buslaps, T., Soloducha, K., 2016. Elastoplastic deformation and damage process in duplex stainless steels studied using synchrotron and neutron diffractions in comparison with a self-consistent model 81, 102–122. https://doi.org/10.1016/j.ijplas.2016.01.018

Zhao, Y., Joncour, L. Le, Baczma, A., Gadali, E., Wro, S., Panicaud, B., François, M., Braham, C., Buslaps, T., 2017. Stress distribution correlated with damage in duplex stainless steel studied by synchrotron diffraction during plastic necking 113, 157–168. https://doi.org/10.1016/j.matdes.2016.10.014